Energy Conversion and Management 279 (2023) 116776

Contents lists available at ScienceDirect

Energy Conversion and Management

journal homepage: www.elsevier.com/locate/enconman

Optimizing printed thermoelectric generators with geometry and processibility limitations

Andres Georg Rösch [a,*], Leonard Franke [a], Md. Mofasser Mallick [a], Uli Lemmer [a,b,c]

[a] Light Technology Institute, Karlsruhe Institute of Technology (KIT), Engesserstrasse 13, 76131 Karlsruhe, Germany
[b] InnovationLab, Speyerer Strasse 4, 69115 Heidelberg, Germany
[c] Institute of Microstructure Technology, Karlsruhe Institute of Technology (KIT), Hermann-von-Helmholtz-Platz 1, 76344 Eggenstein-Leopoldshafen, Germany

A B S T R A C T

Fully printed thermoelectric generators (TEGs) are a promising solution for large scale energy harvesting and waste heat recovery in a broad range of applications. Due to large variations in heat transfer coefficients and temperatures, it is necessary to include these properties of the specific heat source in the design process of the TEGs. Oftentimes, this leads to additional, geometric requirements for the devices. The limited layer thickness of the printing process imposes further limitations on the device geometry. Here, we present an analytical method to design and optimize fully printed TEGs manufactured by a screen-printing technique and considering its geometric design limitations. The design process includes choosing between a planarly printed device architecture and a folded device architecture. Furthermore, the limited device thickness and the presence of a filler material in printed TEGs result in device designs optimized for output power, which vary from conventional thermal impedance matching. The fill factor is hereby an important degree of freedom for the optimization. Furthermore, we demonstrate, that two materials with the same figure of merit zT will yield different output powers for the same device, if their thermal conductivities differ. This implies that considering the geometric limitations of the intended application already in the development of the printable thermoelectric materials can yield a larger power output for the device.

1. Introduction

To reach the global goal of net-zero carbon emissions in the effort to combat climate change, switching the primary energy sources to renewable energies has to be accompanied by an increase of energy efficiency. [1] Scientists estimate that 52 % of global primary energy production is lost in the form of waste heat in exhaust and effluent losses. In 2012 this wasted energy amounted to 68,103 TWh. [2] Recovering this discarded energy even partially by transforming it back into usable electrical energy thereby presents a significant source of energy that would otherwise be unnecessarily released into the environment. The major challenge in waste heat recovery lies in the fact that the unused heat predominantly exists as low temperature thermal energy. [2] This makes it mostly unavailable for conventional heat engines. Furthermore, possible heat sources and heat sinks are of varying shapes and materials ranging widely from hot surfaces in industrial settings to complex geometries in heat exchangers. It is therefore paramount to design for each application an adapted waste heat recovery (WHR) system to achieve maximal power generation.

A promising solution for a broadly usable large scale WHR technology in industrial settings are printed thermoelectric generators [3–12] (TEG). TEGs have a unique ability to convert thermal energy in electrical energy via the Seebeck effect [13] without any moving parts using even very small temperature differences. Conventional, commercially available TEGs are predominantly based on bulk Bi_2Te_3 and have only found use in niche applications. [14,15] The relatively high price of these modules [16] due to its complex manufacturing process impeded their large-scale application as WHR or energy-harvesting systems.

A possible solution are fully printed TEGs made by large-scale screen printing, ink-jet printing, or 3D printing. [17–19] These new additive manufacturing techniques plus recent developments in highly efficient and printable thermoelectric (TE) materials [12,20–26] enable fast and simple manufacturing processes reducing the costs and allow for a potential competitiveness in the market. Furthermore, the easily adjustable manufacturing processes can produce large area and customizable devices adapted to the different shapes and thermal resistances of individual applications.

Small energy-harvesting units powering small devices such as sensors, actuators, and data transmitters are an equally interesting use case for printed TEGs and might find widespread application in wearables and IoT (Internet-of-Things) devices. [27–30].

In this work we present the analytical optimization of fully printed TEGs for maximal output power. While there are already many studies on the general analytical optimization of conventional TEGs, [31–35]

* Corresponding author.
E-mail address: andres.roesch@kit.edu (A.G. Rösch).

https://doi.org/10.1016/j.enconman.2023.116776
Received 4 December 2022; Received in revised form 29 January 2023; Accepted 2 February 2023
Available online 9 February 2023

subject matter of this work are fully printed devices with their geometry and processability limitations. The most significant differences, between printed and conventional TEGs is the need for a substrate material, such as polymer foils, glass fibres, or passivated metal foils as well as dimensionality restrictions dictated by the fabrication process, such as a maximum possible printed layer thickness, a maximum possible fill factor, and a minimum printing resolution. Without loss of generality, we focus on printed TEGs manufactured by a screen printing process conducted in our previous research. [3,21,26,36,37] We will present different device architectures and show which design choices in the TEG layout and the thermoelectric material are necessary to maximize the output power.

The true strength in printed thermoelectric devices, besides potentially low manufacturing cost through largely scalable mass manufacturing (e.g. roll-to-roll manufacturing), is their customization ability. The vast variety of heat sources that can be used for the energy-harvesting of environmental or waste heat require a different device design for almost every application. While the development of printable TE materials with an increasingly high zT value remains the key driver for achieving high energy conversion efficiencies, the device design (e.g. device geometry, choice of substrate material, etc.) occupies an equally important role, once we put the highly efficient printable thermoelectric material to use in a WHR or energy harvesting application.

The performance of a TE material is usually quantified by the unitless figure of merit [38]

$$zT = \frac{\alpha^2 \sigma}{\kappa} T, \tag{1}$$

where α is the material's Seebeck coefficient, σ its electrical conductivity, κ its thermal conductivity, and T the absolute temperature. Hereby, an n-type material has a negative Seebeck coefficient, and a p-type material has a positive Seebeck coefficient. This figure of merit is directly coupled with the maximum conversion efficiency [38]

$$\eta_{\max} = \frac{T_h - T_c}{T_h} \cdot \frac{\sqrt{1+zT}-1}{\sqrt{1+zT}+\frac{T_c}{T_h}}, \tag{2}$$

of a TEG between a hot reservoir with temperature T_h and a cold reservoir with temperature T_c. A TEG typically comprises numerous thermoelectric elements electrically connected in series, alternating between p-type and n-type, and thermally connected in parallel. This way, the Seebeck voltages generated in the elements add up to higher voltages that reduce ohmic losses and can be used more efficiently by a subsequent electronic power management systems.

Aside from using highly efficient TE materials in a device, optimizing the geometry of a TEG is pivotal to either extract the most output power or convert energy with the highest efficiency. To maximize the power flowing into the TEG, its thermal impedance must match the thermal impedances of the heat source and the heat sink. Analogously, to maximize the power flowing from the TEG into the load, the electrical impedance of the TEG must match the electrical impedance of the load.

2. Printed TEG device architectures and design considerations

During the manufacturing of printed TEGs, the thermoelectric materials, and other conductive materials are in the form of printable inks or pastes and deposited in thin films on a usually flexible substrate. There are essentially-two device architectures for 2D-printed thermoelectric devices (Fig. 1). We will distinguish between a planar architecture (Fig. 1**a**), in which different materials are printed on top of each other and the heat flow is cross-plane and a folded (or corrugated) architecture (Fig. 1**b**) in which the materials are printed next to each other and then folded up, resulting in an in-plane heat flow.

The planar architecture is virtually identical to conventional TEGs and Peltier elements, where the substrate and the conductive material acts as an in-series thermal resistance between the heat source/sink and the thermoelectric material, causing an increased thermal contact resistance to the device. Furthermore, planarly printed TEGs might have an additionally printed electrically insulating filler material in between the TE elements for structural support, whereas a conventional TEG has air as filler material. In the folded case the substrate acts as a parallel thermal conductance between the thermoelectric elements, causing parasitic unused heat flow between the heat source and heat sink. In both cases the substrate needs to be an electrical insulator and as thin as possible. However, the planar architecture requires a substrate material with high thermal conductivity (e.g., passivated metal foil or ceramic plates in conventional devices) whilst the folded architecture needs a substrate with a low thermal conductivity (e.g., polymer foil) to minimize detrimental effects on the device's performance.

Apart from using printable thermoelectric materials with the highest zT possible, manufacturing a high performing device requires an optimization of its geometric dimensions. The effective ZT value of the device (and therefore its efficiency) as well as its output power are strongly dependent on the cross-section areas and the lengths of the TE elements

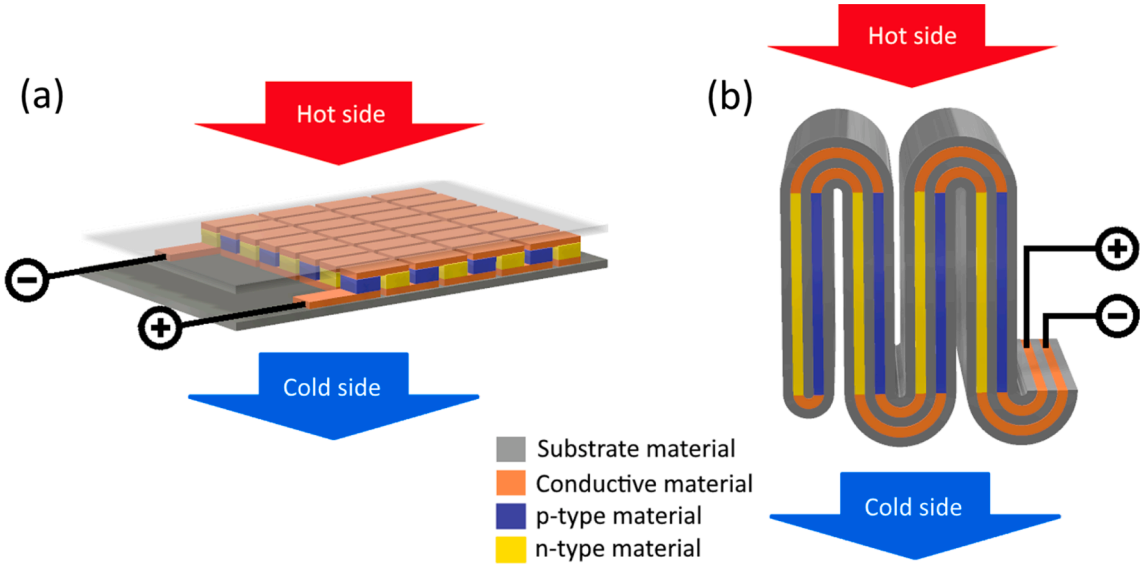

Fig. 1. Schematic of device architectures for printed thermoelectric generators. (a) Printed planar (thin film) TEG with the substrate thermally in series to thermoelectric material. (b) Origami folded TEGs with a corrugated device architecture and the substrate thermally in parallel to thermoelectric material.

(or legs), as well as the devices fill factor, defined as the ratio between the sum of all cross-section areas of the TE elements and the total cross-section area of the device.

Due to the presence of a filler material and a substrate with a non-negligible thermal conductivity, the influence of the fill factor becomes more prominent in printed TEGs compared to conventional devices. Furthermore, in the case of printed TEGs, the device's thickness is often limited by either the manufacturing process (e.g., minimal, or maximal printable layer thickness or foldable leg length) or by geometric limitations in the application (e. g. max. acceptable thickness for wearables). Therefore, the fill factor becomes an important degree of freedom in the design and optimization of a printed TEG. Previous analytical optimizations of conventional TEGs found in literature have typically assumed air as the filler material, with a very low thermal conductivity of $0.015\,\mathrm{Wm^{-1}K^{-1}}$. [31,33,34] This value is usually neglected (by rounding it down to zero) since it is small compared to the thermal conductivities of the TE materials. This approximation is not justifiable for printed TEGs.

Therefore, in the following sections, we will derive the analytical expressions for the effective ZT value and the maximum output power as a function of the geometric parameters, particularly the device's fill factor. We will neglect parasitic non-linear radiative and convective heat transport as theses effect are minor importance in the presence of a filler material. [39,40] It allows an analytical approach to the optimization, demonstrating the principles at hand.

3. The fill factors influence on the effective Z

Fig. 2**a** shows a typical arrangement of two TE legs in a conventional or planarly printed thermocouple. The material properties of the n- and p-type TE materials are $\alpha_n, \sigma_n, \kappa_n$ and $\alpha_p, \sigma_p, \kappa_p$, respectively. Through the applied temperature difference $\Delta T = T_h - T_c$ the TE device generates a proportional voltage $V_{oc} = (\alpha_p - \alpha_n)\cdot\Delta T$. We consider the total cross-section area of the device A, the effective area of the TE material $A_{TE} = A_n + A_p = FA$, and the passive area $A_{filler} = A(1-F)$ filled by a filler material with the thermal conductivity κ_{filler}. Here, F is the fill factor of the TE device. A_p and A_n are the cross-section areas of the leg. The length (or thickness) of the n-type TE leg, p-type TE leg, the filler material, and the whole device are d_n, d_p, d_{filler}, and d respectively. A thermocouple in a folded TEG (Fig. 2**b**) lies thermally in parallel with the substrate. The non-active cross-section area consists of the sum of the cross-sections of the substrate (with κ_{sub}) and the air gap (with κ_{gap}) between the printed elements $A_{filler} = A_{sub} + A_{gap} = A(1-F)$. In this case we have an effective thermal conductivity of $\kappa_{filler} = (\kappa_{sub}\cdot A_{sub} + \kappa_{gap}\cdot A_{gap})/A_{filler}$.

The effective Z of a TE device is defined as: [41]

$$Z = \frac{\alpha^2\sigma}{\kappa} = \frac{n^2\cdot(\alpha_p - \alpha_n)^2}{RK}, \tag{3}$$

where n is the number of thermocouples, R the electrical resistance of the device and K the thermal conductance of the device. α, σ, and κ are now the effective material properties of the device. For the effective ZT value, Z is multiplied by the average temperature $T_m = (T_h + T_c)/2$. Unlike the material figure of merit zT in Eq. (1), the effective Z (or ZT) of a device is *not* independent of geometric dimensions. It reaches its maximum value when the product RK is minimal.

In Supplementary Information Note 1, we derived a generalized formula for the maximum effective Z value by calculating the product RK as a function of F and κ_{filler} and minimizing it. This resulted in the generalized geometry condition for the maximum effective Z:

$$\frac{d_p A_n}{d_n A_p} = \sqrt{\frac{\frac{\kappa_p}{\sigma_n} + \frac{d_p\kappa_{filler}}{d_{filler}\sigma_n}\cdot\frac{1-F}{F}}{\frac{\kappa_n}{\sigma_p} + \frac{d_n\kappa_{filler}}{d_{filler}\sigma_p}\cdot\frac{1-F}{F}}}. \tag{4}$$

We can then write the resulting expression for the maximum effective Z value as:

$$Z_{max} = \frac{(\alpha_p - \alpha_n)^2}{\left(\sqrt{\frac{\kappa_n}{\sigma_n} + \frac{d_n\kappa_{filler}}{d_{filler}\sigma_n}\cdot\frac{1-F}{F}} + \sqrt{\frac{\kappa_p}{\sigma_p} + \frac{d_p\kappa_{filler}}{d_{filler}\sigma_p}\cdot\frac{1-F}{F}}\right)^2} \tag{5}$$

In the case of $F = 1$ (no gap between the TE elements) or $\kappa_{filler} = 0$ (the thermal conductivity of the filler material is negligible) Eq. (4) and Eq. (5) become:

$$\frac{d_p A_n}{d_n A_p} = \sqrt{\frac{\sigma_p\kappa_p}{\sigma_n\kappa_n}} \tag{6}$$

and

$$Z_{max} = \frac{(\alpha_p - \alpha_n)^2}{\left(\sqrt{\frac{\kappa_n}{\sigma_n}} + \sqrt{\frac{\kappa_p}{\sigma_p}}\right)^2} \tag{7}$$

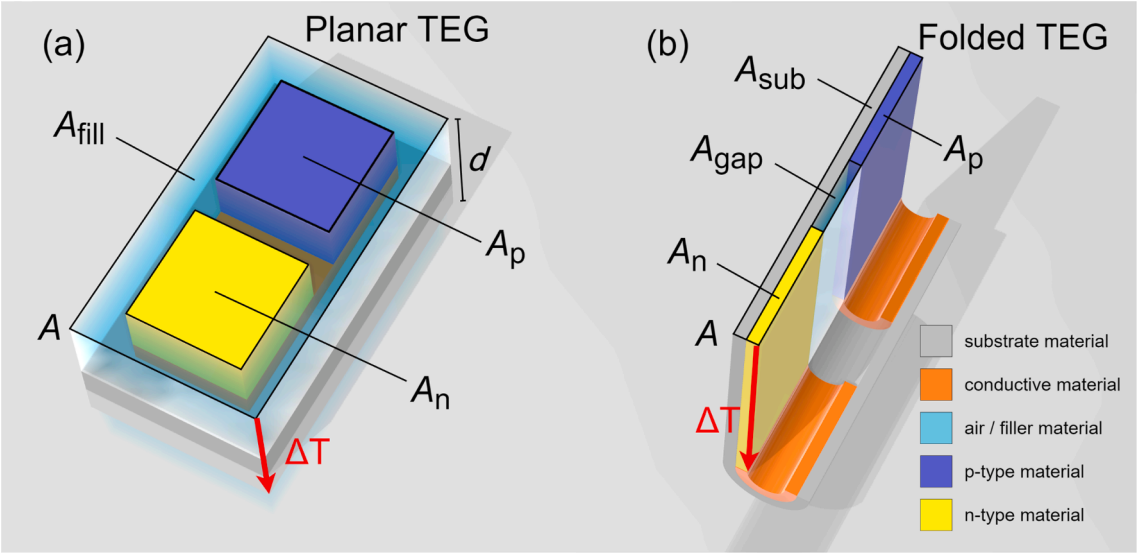

Fig. 2. Schematic of a thermocouple within a printed TEG (a) Planarly printed thermocouple between two substrate layers. (b) Folded thermocouple thermally in parallel with one layer of substrate material. The space between the thermoelectric elements is filled with a filler material. The red arrows indicate the applied temperature difference ΔT that generates a voltage V_{oc} across the elements. (For interpretation of the references to colour in this figure legend, the reader is referred to the web version of this article.)

respectively. Eq. (6) and Eq. (7) are well known equations and agree with the general textbook knowledge for thermoelectric devices. [41].

For the majority of applications a flat interface of the device to the heat source and heat sink is advantageous. Therefore we can choose $d_p = d_n = d_{filler} = d$ so that Eq. (4) and Eq. (5) reduce to

$$r := \frac{A_n}{A_p} = \sqrt{\frac{\frac{\kappa_p}{\sigma_n} + \frac{\kappa_{filler}}{\sigma_n}\frac{1-F}{F}}{\frac{\kappa_n}{\sigma_p} + \frac{\kappa_{filler}}{\sigma_p}\frac{1-F}{F}}} \tag{8}$$

an expression of the ratio r between the cross-section areas with $r = A_n/A_p$ and

$$Z_{max} = \frac{(\alpha_p - \alpha_n)^2}{\left(\sqrt{\frac{\kappa_n}{\sigma_n} + \frac{\kappa_{filler}}{\sigma_n}\frac{1-F}{F}} + \sqrt{\frac{\kappa_p}{\sigma_p} + \frac{\kappa_{filler}}{\sigma_p}\frac{1-F}{F}}\right)^2}. \tag{9}$$

Using r calculated according to Eq. (8), we can then derive general expressions for the optimal cross-section areas A_n and A_p to:

$$A_n = \frac{FA}{n\left(\frac{1}{r}+1\right)}, A_p = \frac{FA}{n(r+1)}. \tag{10}$$

As presumed, in the general case with the filler material, the effective Z value decreases with decreasing fill factor or increasing κ_{filler} since we introduce more parasitic heat flow through the device. It is therefore essential that we choose κ_{filler} as small as possible, as long as other choosing criteria e.g. mechanical, thermal, and chemical stability or wettability are met.

Regarding the effective material properties of the device, we can express them as follows:

The effective Seebeck coefficient

$$\alpha = n\cdot(\alpha_p - \alpha_n), \tag{11}$$

the effective electrical conductivity

$$\sigma = \frac{1}{R}\frac{d}{A} = \frac{1}{n\cdot(R_n + R_p)}\frac{d}{A} = \frac{F}{\frac{\left(\frac{1}{r}+1\right)}{\sigma_n} + \frac{(r+1)}{\sigma_p}}, \tag{12}$$

and the effective thermal conductivity

$$\kappa = K\cdot\frac{d}{A} = n\cdot(K_n + K_p + K_{filler})\cdot\frac{d}{A} = \left(\frac{\kappa_n}{\left(\frac{1}{r}+1\right)} + \frac{\kappa_p}{(r+1)}\right)\cdot F + \kappa_{filler}\cdot(1-F). \tag{13}$$

The energy conversion efficiency η of a TEG is monotonically coupled with the effective Z via Eq. (2). Therefore maximizing the Z value implies maximizing the device efficiency.

4. The fill factor's influence on the maximum output power

Maximizing the output power of a TEG in an energy-harvesting application usually requires simultaneous thermal impedance matching of the device to the heat source and heat sink and electrical impedance matching to the load. This maximizes the thermal energy flow from the heat source into the device and the electrical energy flow from the device to the load. Fig. 3 shows an equivalent circuit diagram of a TEG in use developed by Yazawa and Shakouri. [33] On the thermal side, the TEG lies between the heat source with the thermal conductance K_h at the temperature T_s and the heat sink with the thermal conductance K_c at the ambient temperature T_a. Hereby, K_h and K_c are the series connection of all thermal conductances and heat transfer coefficients along the heat flow on the hot and the cold side respectively. T_h and T_c are the temperatures at the hot and the cold side of the TEG. Apart from the heat flow coming from the heat source, the Peltier effect ($-\alpha I T_h$ and $\alpha I T_c$ to the hot side and cold side respectively) and Joule heating ($1/2RI^2$ to each side) resulting from the electrical current I through the device

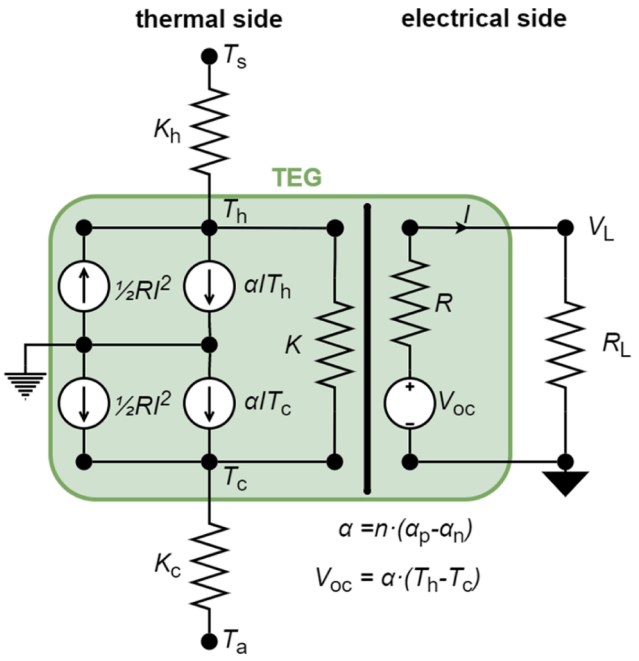

Fig. 3. Thermal and electrical equivalent circuit diagram (ECD) of a TEG. On the thermal side, the components represent the thermal conductances of the heat source and heat sink and their respective temperatures. Inside the TEG, Joule heating and the Peltier effect are represented by heat flow sources and thermal conduction by a conductance. On the electrical side the Seebeck effect is modeled by a voltage source with internal resistance connected to a load resistance. The ECD was developed by Yazawa and Shakouri [33].

are further heat flow contributions represented by additional heat flow sources. On the electrical side, the TEG powers an application with the electrical resistance R_L.

In most applications, we cannot adapt the heat source, since it is fixed by external parameters such as dimensions, flow rate, temperature, etc., as it often serves another purpose as e.g., heaters, coolers, pipes, or heat exchangers. The heat sink on the other hand serves to increase the heat transfer from the TEG to the environment. It is, therefore, necessary to choose a heat sink with maximum K_c allowing a high heat flow through the TEG. The most feasible way of achieving the thermal impedance matching is to adapt the thermal conductance K of the TEG via its thickness determined by leg length d. To calculate the output power per unit area we need to replace K_h and K_c by the heat transfer coefficients (HTC) k_h and k_c of the heat source and heat sink interfaces. We can recalculate the thermal conductances by $K_h = k_h\cdot A$ and $K_c = k_c\cdot A$.

Yazawa and Shakouri published a comprehensive discussion of the influence of the device thickness d of a TEG on its maximal output power. [33] They derived expressions for the heat flux $\dot{q}_h$ into and the heat flux $\dot{q}_c$ out of the device with:

$$\dot{q}_h := k_h(T_s - T_h) = \frac{\kappa}{d}\left(1 + \frac{Z}{2(1+m)^2}((2m+1)T_h + T_c)\right)(T_h - T_c) \tag{14}$$

and

$$\dot{q}_c := k_c(T_c - T_a) = \frac{\kappa}{d}\left(1 + \frac{Z}{2(1+m)^2}((2m+1)T_c + T_h)\right)(T_h - T_c) \tag{15}$$

Furthermore the output power per unit area of the TEG can be calculated with: [33]

$$w = \dot{q}_h - \dot{q}_c = \frac{I^2 mR}{A} = \frac{mZ}{(1+m)^2}\frac{\kappa}{d}(T_h - T_c)^2, \tag{16}$$

where $m = R_L/R$ is the ratio between the load resistance R_L and the

electrical resistance R of the device, Z is the device figure of merit of Eq. (3) and κ the effective thermal conductivity of Eq. (13).

After co-optimizing Eq. (16) with respect to m and d to achieve maximal output power (thermal and electrical impedance matching), Yazawa and Shakouri derived the optimal device thickness

$$d_{opt} = \kappa \frac{k_h^{-1}(T_h + (2m-1)T_c) + k_c^{-1}((2m-1)T_h + T_c)}{(T_h + T_c)}. \quad (17)$$

Here, m has to be simultaneously co-optimized. This yields

$$m_{opt} = \sqrt{1+ZT} \quad (18)$$

for the optimal resistance ratio.

Therefore, we achieve the maximum output power per unit area by inserting d_{opt} and m_{opt} in Eq. (16):

$$w_{max} = \frac{m_{opt} Z_{max}}{(1+m_{opt})^2} \frac{\kappa}{d_{opt}} (T_h - T_c)^2. \quad (19)$$

To calculate w_{max}, however, the temperatures at the TEG T_h and T_c are needed. These are unknown entities, unlike the given boundary temperatures T_s and T_a of heat source and heat sink. We can calculate T_h and T_c via a system of two implicit simultaneous equations (Eq. (15) and Eq. (17) in Ref. [33]) derived by Yazawa and Shakouri, however solving the system of equation requires numerical solving due to its complexity. [33]

In the case of a negligible $\kappa_{filler} \approx 0$, the maximum output power w_{max}, is independent of the fill factor. This stems from the fact that for $\kappa_{filler} \approx 0$ the term Z_{max} obeys Eq. (9) and is independent of the fill factor. Furthermore, κ and d_{opt} are both proportional to the fill factor and its influence cancels out in Eq. (19).

This means that the device can have a low fill factor without the loss of output power. This allows reducing the volume and therefore the cost of used thermoelectric material by F^{-2} without changing the thermoelectric properties of the generator. [31,34,42].

Eq. (19) is valid for the general case with or without filler material. The independence of w_{max} from the fill factor does not apply in the case of a filler material with $\kappa_{filler} > 0$. Then Z_{max} becomes dependent on F according to Eq. (9) and the output power decreases with decreasing fill factor.

5. Discussion

After assessing the exact influence of the fill factor onto the different effective thermoelectric properties and geometric dimensions, we can now use the model to answer several questions related to the design and the performance of printed TEGs. For quantitative calculations we choose as material properties the properties of printable thermoelectric inks developed by our group and published by Mallick et al.. [26,43] We list the materials properties in Table 1.

5.1. Question 1: To fold or not to fold?

Using a film deposition technology like printing limits the possible layer thickness and therefore the possible device thicknesses for planar TEGs. On the other hand, folded TEGs have a lower limit for the device thickness due to limitations in the printing resolution and the foldability / flexibility of the substrate. Without loss of generality, we take 100 μm as the highest possible thickness printable with a conventional screen-printing process and therefore the largest device thickness possible for planar TEGs with the device architecture of Fig. 1**a**. On the other hand, we assume that 1 mm is the lowest possible device thickness for a folded TEG with the device architecture of Fig. 1**b** printed by screen printing, since it becomes very challenging to fold below this value.

Table 1
Material properties of printable thermoelectric materials at room temperature (303 K).

	BiSbTe ink [43]	**Ag_2Se ink** [26]
Type	p-type	n-type
Electrical conductivity (S/cm)	447	460
Seebeck coefficient (μV/K)	198	−191
Thermal conductivity ($Wm^{-1}K^{-1}$)	0.45	0.50
Power factor ($\mu Wm^{-1}K^{-2}$)	1760	1680
zT value	1.18	1.03

A closer look to the optimal device thickness d_{opt} in Eq. (17) reveals that it mainly depends on k_h and k_c, since they are inversely proportional to d_{opt} and can vary from some tens of $W/(m^2K)$ for wearable applications using the human body as a heat source and the surrounding air as a heat sink to several thousand of $W/(m^2K)$ for waste heat recovery applications where TEGs are integrated inside high-efficient water based heat exchangers. Determining k_h and k_c as precisely as possible for each application either by measurement or simulation is crucial for designing a high performing TE device. In this work we will look at two exemplary scenarios. Application I is a wearable device [35] with $k_h = 50$ $W/(m^2K)$ and $k_c = 10$ $W/(m^2K)$. As Application II, we will choose a water-to-water plate heat exchanger [44] with a very high overall heat transfer coefficient (U-value) of 4000 $W/(m^2K)$. For simplicity, we assume equal thermal conductance for both sides and no significant influence on them by the installed TEG, therefore $k_h = k_c = 8000$ $W/(m^2K)$.

The influence of the temperatures T_h and T_c on d_{opt} on the other hand is significantly smaller. For an initial general analysis of the device thickness, we will therefore choose the fixed temperatures of $T_s = 350$ K and $T_a = 300$ K.

Fig. 4 shows the optimal device thickness d_{opt} as a function of the total heat transfer coefficient on the hot side k_h and the total heat transfer coefficient on the cold side k_c for three different F-κ_{filler}-combinations. As a consequence of the serial connection of heat source device and heat sink d_{opt} is strongly dependent on k_h and k_c. In the cases where k_h and k_c vary strongly from one another d_{opt} is mainly dependent on the significantly lower heat transfer coefficient. Therefore the parameter space of the k_h-k_c plane is divided roughly by the $k_h = k_c$ line into two triangular domains where either k_h or k_c is dominant for the determination of the optimal device thickness.

Fig. 4**a** displays the case for a device with 100 % fill factor ($F = 1$, κ_{filler} arbitrary), which yields the highest possible output power for both applications since it reaches maximal effective Z values. No filler material implies the need of a planarly printed (non-folded) device architecture. We marked as red dashed line the 100 μm line as our maximum printable layer thickness and hatched with diagonal lines all possible HTC combinations attainable with screen-printed planar device. Furthermore, we marked the above mentioned Applications I and II as red stars and calculated their respective optimal device thicknesses and their maximal power densities. Application I (wearable) requires a device thickness of 8.5 cm to reach the maximal output power of 3.1 W/m^2 and Application II (water/water heat exchanger) needs a device thickness of 175 μm for 1.5 kW/m^2. We can clearly see that screen-printing of a planar thermally impedance matched device is not possible for any of the two applications, since we cannot reach the required device thicknesses with the 100 μm layer thickness limit. It is here where we can exploit the fill factor to compensate for the processibility limitations.

Fig. 4**b** shows the same d_{opt} for $F = 0.1$ with air ($\kappa_{filler} = 0.015$ W/(mK)) as a filler material. Reducing the fill factor results in a smaller d_{opt} and we can realize a thermally impedance matched planar device with only 21 μm in thickness for the heat exchanger application. The low κ_{filler} limits the loss of output power to only down to 1.2 kW/m^2. Note that the device generates this output power with only 1.2 % of the volume of TE material compared to the case of $F = 1$, which shows the reduction in material usage. This effect can be used to optimize the $ per Watt metric of TEGs. [31,32,34] The Application I as a wearable device also benefits from a reduction in device thickness for a better form factor. An 8.5 cm thick device as for $F = 1$, while being optimal for performance, is too

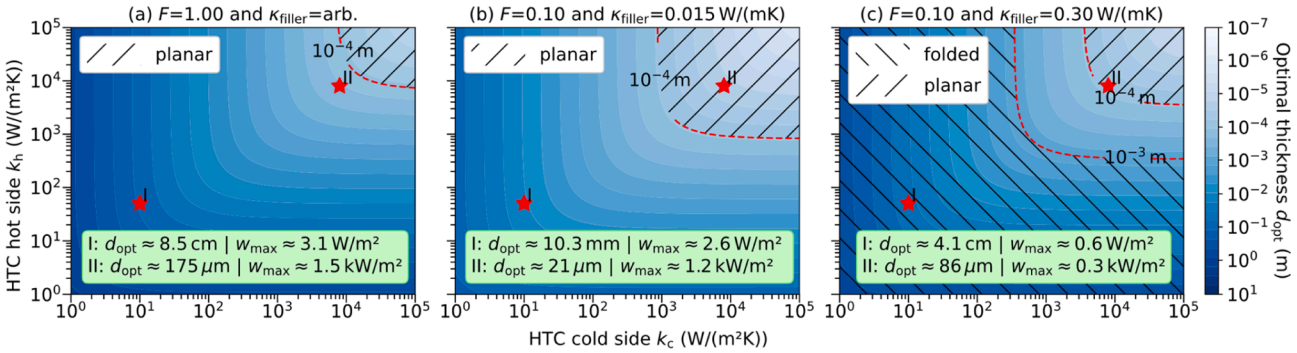

Fig. 4. Optimal device thickness for printed TEGs. Optimal device thickness as a function of the heat transfer coefficients (HTC) of the heat source and heat sink for different fill factors and filler materials. a) $F = 1$, κ_{filler} = arb., b) $F = 0.1$, $\kappa_{filler} = 0.015$ W/(mK), c) $F = 0.1$, $\kappa_{filler} = 0.3$ W/(mK). The red stars mark a wearable energy-harvesting application (I), a waste heat recovery application in a heat exchanger (II). The respective optimal device thicknesses and output power densities are given in the green text boxes. The hatched areas indicate which applications can be realized by a planar and a folded device architecture, respectively. (For interpretation of the references to colour in this figure legend, the reader is referred to the web version of this article.)

bulky and hardly comfortable as a wearable device. For $F = 0.1$ the device thickness reduces to only 10.3 mm, which can be worn more comfortably, while still having a good performance of 2.6 W/m^2. This reduced device thickness, however, still exceeds the maximal layer thickness to realize it with the planar architecture. It is therefore necessary for applications with low thermal contact resistances to use a folded architecture to reach the required higher device thicknesses. However, the thermally parallel substrate will significantly increase κ_{filler}.

Fig. 4**c** shows the optimal device thickness for $F = 0.1$ and an increased $\kappa_{filler} = 0.3$ W/(mK). We have additionally marked the area of HTC combinations that can be attained by folded devices with a minimum thickness of 1 mm. This includes Application I. The gap between the hatched areas indicates HTC combination for which we cannot fabricate an optimized device with this screen-printing method, neither planar nor folded. However, these applications might be suited by other thick film or 3D printing techniques. The higher κ_{filler} in combination with the low fill factor has a significant impact on the output power, reducing it to 0.6 W/m^2 for Application I and to 0.3 kW/m^2 for Application II. Furthermore, the optimal device thicknesses increase again to 4.1 cm and 86 μm respectively due to the increase in the effective κ. As most applications for wearables and energy-harvesting exhibit low HTCs, we conclude that suitable TEGs can be realized with a folded architecture. [45] Waste heat recovery systems in heat exchangers on the other hand are realizable with planarly printed devices and a reduced fill factor.

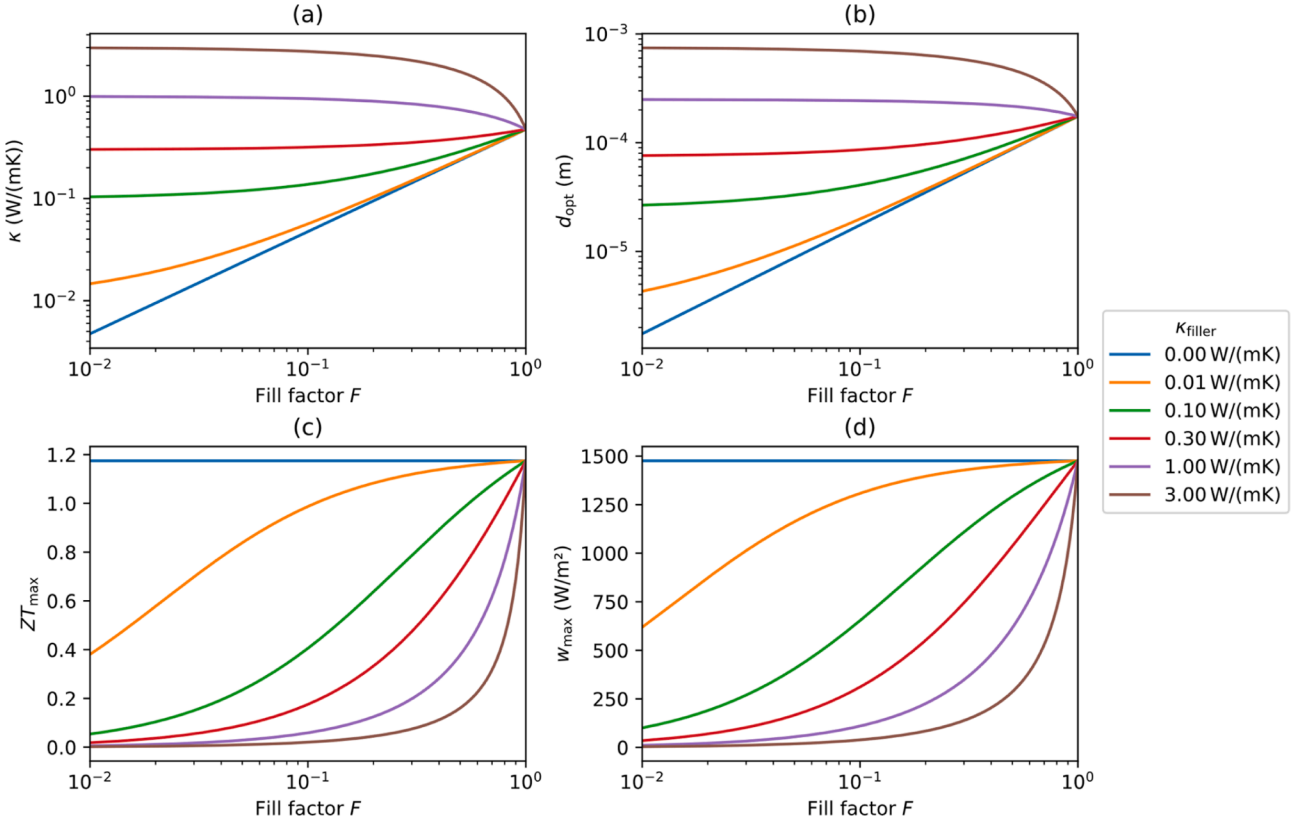

Fig. 5. Device properties of an impedance matched device in a heat exchanger application a) Effective thermal conductivity, b) optimal device thickness, c) effective ZT value, d) maximal output power density for different filler materials as a function of the fill factor.

5.2. Question 2: Is thermal impedance matching necessary?

We showed that when geometric requirements or the manufacturing processes limit the device thickness, we can achieve thermal impedance matching by tuning the optimal device thickness d_{opt} via the fill factor. However, this possibility diminishes with increasing κ_{filler}. Fig. 5 shows κ, d_{opt}, ZT_{max}, and w_{max} for Application II (integration in a heat exchanger) as a function of the fill factor for a variety of values for κ_{filler}. Reducing the fill factor causes the κ to converge towards κ_{filler} (Fig. 5**a**), which in return causes the optimal thickness d_{opt} to level off for small fill factors (Fig. 5**b**). This limits the ability to use the fill factor to adjust the optimal device thickness if a filler material with a significant κ_{filler} is present. Furthermore, Z_{max} (and therefore ZT_{max} in Fig. 5**c**) and consequently w_{max} (Fig. 5**d**) drop rapidly for smaller fill factors and higher κ_{filler}. It is interesting to note that we can compensate for a reduction in the effective ZT due to a large κ_{filler} with a higher fill factor. This is particularly important while comparing folded to planar devices, since folded devices usually have a high κ_{filler}, but can achieve high fill factors if thin substrates are used [3].

To understand the principles for the design of a thin film device with a limited leg length, we plotted the output power density w (Eq. (16)) as a function of d and F for Application II for $\kappa_{filler} = 0.0$ W/(mK) (Fig. 6**a**), $\kappa_{filler} = 0.015$ W/(mK) (Fig. 6**b**), $\kappa_{filler} = 0.1$ W/(mK) (Fig. 6**c**), and $\kappa_{filler} = 0.3$ W/(mK) (Fig. 6**d**). With a known device thickness d, we must calculate T_h and T_c by numerically solving the simultaneous heat flux equations Eq. (14) and Eq. (15) for T_h and T_c. Furthermore, we indicate as a red line all d-F-tuples for which the resulting TEG is thermally impedance matched, therefore being $d_{opt}(F)$. The blue line indicates the thickest possible planar devices with a device thickness of 100 μm while the green line sets the lower limit of 1 mm for the folded devices. We can see that in all cases the maximum output power lies at $d = d_{opt}, F = 1$. For $\kappa_{filler} = 0.0$ W/(mK), however, the maximum output power can be achieved at all points on the red line indicating impedance matching.

For a non-vanishing thermal conductivity of the filler materials ($\kappa_{filler} > 0$), w drops along the red line with decreasing F due to the decrease in the effective Z. This effect becomes more prominent with increasing κ_{filler}. Furthermore, devices along the green line that cannot reach thermal impedance matching because their possible leg thickness is too large always need to maximize their fill factor for the highest output power. This is due to the monotonic increase of w for increasing F ($\partial w/\partial F > 0$) for all $d > d_{opt}$.

However, in most real applications, the non-trivial case $d < d_{opt}$ applies, due to the thickness limit for planar devices. In this case, w is not monotonically decreasing with decreasing F. We can see that it is possible to manufacture a planar device with a limited leg length of 100 μm (blue line) that is thermally impedance matched, by choosing F such that the device lies on the intersection between the blue and the red curve. However, while these devices maximize the $\Delta T = T_h - T_c$, due to a reduced effective Z with a low F, the maximum power point differs from this intersection. Table 2 lists several devices along the blue 100 μm lines in Fig. 6 where the *italic* entries are impedance matched and the **bold** entries are the points of maximum output power. For $\kappa_{filler} = 0.0$ W/(mK), both points are at $F = 0.572$. Due to the relatively large thermal conductivities of the TE materials, a reduced fill factor results in an increase of ΔT to 25 K. However, with increasing κ_{filler} the maximum power point moves to larger fill factors, since the increase in ΔT is counteracted by the decrease in effective Z. While for air ($\kappa_{filler} = 0.015$ W/(mK)) as a filler material, the maximum power point deviates only slightly from the point indicating thermal impedance matching. For $\kappa_{filler} = 0.1$ W/(mK) we already need to set the fill factor to $F = 0.836$ to get 1377 W/m^2 with a reduced ΔT of 20.0 K compared to the 1289 W/m^2 at the thermal impedance matching point with a ΔT of 25 K. For even larger $\kappa_{filler} = 0.3$ W/(mK), the maximum power point of 1366 W/m^2 moves all the way to a fill factor of $F = 1$, while the thermal impedance matched device at $F = 0.232$ produces only 618 W/m^2. For any filler material with an even larger thermal conductivity, the optimum fill

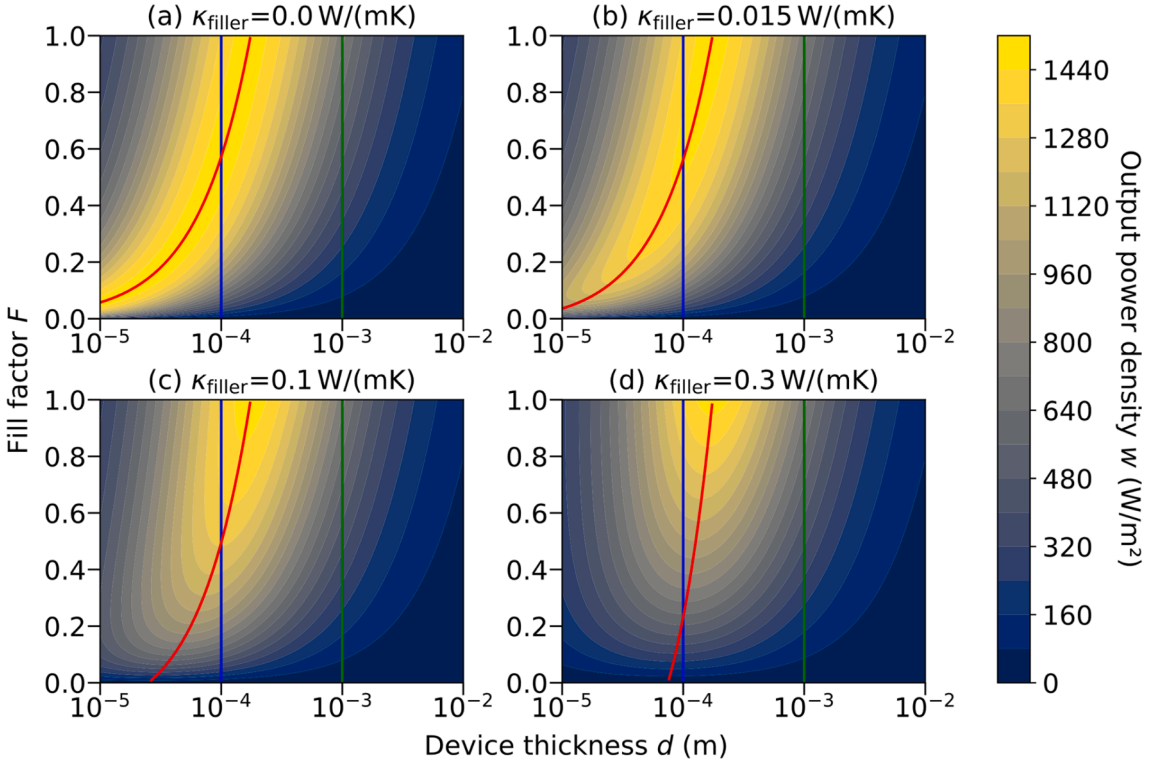

Fig. 6. Output power density for a printed TEG in a heat exchanger application. Output power density as a function of fill factor and device thickness for different filler materials with a) $\kappa_{filler} = 0$ W/(mK), b) $\kappa_{filler} = 0.015$ W/(mK), c) $\kappa_{filler} = 0.1$ W/(mK), and d) $\kappa_{filler} = 0.3$ W/(mK). Red line: devices that meet the impedance matching condition, blue line: planar TEGs with the highest thickness (100 μm), green line: thinnest folded TEGs with 1 mm device thickness. (For interpretation of the references to colour in this figure legend, the reader is referred to the web version of this article.)

Table 2
Device properties for the thin film heat exchanger application for different filler materials and fill factors.

κ_{filler}(W/(mK))	d(μm)	F	Z(K^{-1})	ZT@325K	ΔT(K)	w(W/m^2)
0	***100***	***0.572***	***3.62 × 10^{-3}***	***1.175***	***25.0***	***1476***
0.015	*100*	*0.562*	*3.53 × 10^{-3}*	*1.147*	*25.0*	*1452*
0.015	**100**	**0.606**	**3.54 × 10^{-3}**	**1.151**	**24.1**	**1454**
0.015	100	1	3.62 × 10^{-3}	1.175	18.2	1366
0.1	*100*	*0.490*	*2.97 × 10^{-3}*	*0.967*	*25.0*	*1289*
0.1	**100**	**0.836**	**3.47 × 10^{-3}**	**1.128**	**20.0**	**1377**
0.1	100	1	3.62 × 10^{-3}	1.175	18.2	1366
0.3	*100*	*0.232*	*1.17 × 10^{-3}*	*0.380*	*25.0*	*618*
0.3	**100**	**1**	**3.62 × 10^{-3}**	**1.175**	**18.2**	**1366**

factor equals 1 for the highest output power.

We can conclude that if the leg thickness is limited by either geometric or process limitations and d_{opt} for $F = 1$ cannot be manufactured, a thermal impedance matched device does not necessarily deliver the maximum output power. Instead, we should choose d as close to the optimum as possible and use the fill factor as a degree of freedom to maximize w.

5.3. Question 3: What is role of κ_p and κ_n?

Lastly, geometric limitations of the device pose special requirements for the printed TE materials. The difficulty to set thermal impedance matching by adjusting the device thickness, can be compensated by selecting the thermoelectric material (among those with high ZT) with a thermal conductivity of the printed layers matched to the application. Knowing k_h and k_c and the aimed device thickness before the selection of the materials can therefore improve the overall performance later on. The materials from Ref. 2 and Ref. 6 were synthesized by mixing elemental powders in a conventional ball milling process. By changing the composition, we can adjust the resulting thermoelectric properties of the composite. [46] This presents an additional degree of freedom to optimize the power output of the TEG. This possibility is discussed in the following. In Eq.1, the zT value remains unchanged if the power factor $\alpha^2\sigma$ and the thermal conductivity κ are both scaled by the same factor s:

$$zT = \frac{\alpha^2\sigma}{\kappa}T = \frac{s\cdot\alpha^2\cdot\sigma}{s\cdot\kappa}T, \tag{20}$$

We can calculate the device performance for different materials with equal zT but different κ values. To simplify the model, we take the TE properties of the BiSbTe ink from Table 1 for p-type and the same properties with opposite signed Seebeck coefficient as n-type material as reference and scale the electrical and thermal conductivities both by s. The Seebeck coefficient remains unchanged. Furthermore, we keep all other parameters the same to calculate an optimum material for the planar device ($d = 100$ μm) integrated into the heat exchanger (Application II). Fig. 7 shows the device properties as a function of the thermal conductivity of the TE material κ_{TE} for different values of κ_{filler}. We marked the properties of the reference device as a vertical red dashed line. The blue dashed line represents the devices, that are impedance matched for $\Delta T = 25$ K and where w is maximized for different κ_{TE}, while keeping the thickness constant at $d = 100$ μm.

We calculated the optimum fill factor of the devices (Fig. 7**a**) by maximizing w numerically with respect to F. $F = 1$ is beneficial when κ_{TE} is small and heat flow through the device is limited. For κ_{TE} higher than the optimum value κ_{im} at impedance matching, smaller fill factors yield higher output power values as this maintains a higher ΔT across the device. The resulting effective thermal conductivity, the effective electrical conductivity, and the effective ZT of the devices are shown in Fig. 7**b**, Fig. 7**c** and Fig. 7**d,** respectively. Furthermore, we plotted the resulting temperature difference (Fig. 7**e**) and finally the output power (Fig. 7**f**). With the reference BiSbTe material ($\alpha_{ref} = \pm$ 198 μV/K, $\sigma_{ref} =$ 447 S/cm, $\kappa_{ref} = 0.45$ W/(mK)), we could achieve an output power of $w_{ref} = 1448$ W/m^2 at $\Delta T = 18.6$ K by choosing $F = 1$. However, tuning the material towards lower thermal and electrical conductivities to hit the thermal impedance matching point, which we calculated to be $\alpha_{im} = \pm$ 198 μV/K, $\sigma_{im} = 264$ S/cm, $\kappa_{im} = 0.27$ W/(mK) we could achieve an output power of $w_{im} = 1551$ W/m^2 at $\Delta T = 25$ K. We can therefore conclude that this material, while having the same zT-value as the BiSbTe ink, would perform 7.1 % better in a planar device of 100 μm thickness installed in the heat exchanger.

Note that F, κ, ZT, ΔT and w in Fig. 7 show no difference between scaling σ by s or scaling α by $\sqrt{s}$ in Eq. (20). While the zT value is important when optimizing an ink, in addition the resulting thermal conductivity can offer an additional degree of freedom in the case of restricted device thicknesses.

Printable thermoelectric inks usually consist of a base thermoelectric material, a binder material, a nano solder material, and a solvent. [21] While the solvent evaporates during the drying process, the thermoelectric material, the binder material, the nano solder remain in the final printed film. To obtain a material with optimized zT and κ, the first and most crucial step is to choose a base thermoelectric material with suitable bulk properties in the temperature range of the desired application. This can either be done scanning large material databases like e.g. The Materials Project [47], for which machine learning algorithms also can be applied to recommend suitable candidates. [48] Material classes such as Chalcogenides, Skutterudites, and Half-Heusler alloys contain a large number of suitable candidates. [49] However, the transformation of these materials into efficient and well-printable inks remains a challenge that requires a trial and error approach. Furthermore, the base material properties can be tuned via doping in order to change its charge carrier concentration. While the electrical conductivity as well the electronic component of the thermal conductivity are linearly proportional to the charge carrier concentration, the Seebeck coefficient has a negative correlation to it. [22] The charge carrier concentration can therefore be used as an additional way to optimize the material. Lastly a printed thermoelectric film is always a multi-phase composite material whose effective electrical thermal and thermoelectric properties result from the volume fraction and the corresponding material property of each subphase. The effective material properties hereby follow the generalized effective medium theory. [46] Through the variation of the composition (e.g. thermoelectric material vs binder material) we can tune e.g. the thermal conductivity to improve the performance of the device further.

6. Conclusion

The extensive development and installation of TEGs for energy-harvesting and waste heat recovery requires the precise dimensioning of a new device design for every application based on the available temperatures and heat transfer coefficients of heat source and heat sink and their geometric shape and dimensions. Additive manufacturing techniques such as printing, in combination with a digital twin are therefore predestined to be the method of choice for easily customizable mass manufacturing of printed TEGs. We presented a full design and optimization process of printed TEGs with a limited device thickness due to geometric or process limitations. Starting with the choice between a folded and a planar device architecture, we can use the fill factor as a degree of freedom to optimize the device performance. We showed that in some cases when a filler material is present, it is beneficial to optimize the device through a numerical optimization for optimum output power rather than for thermal impedance matching.

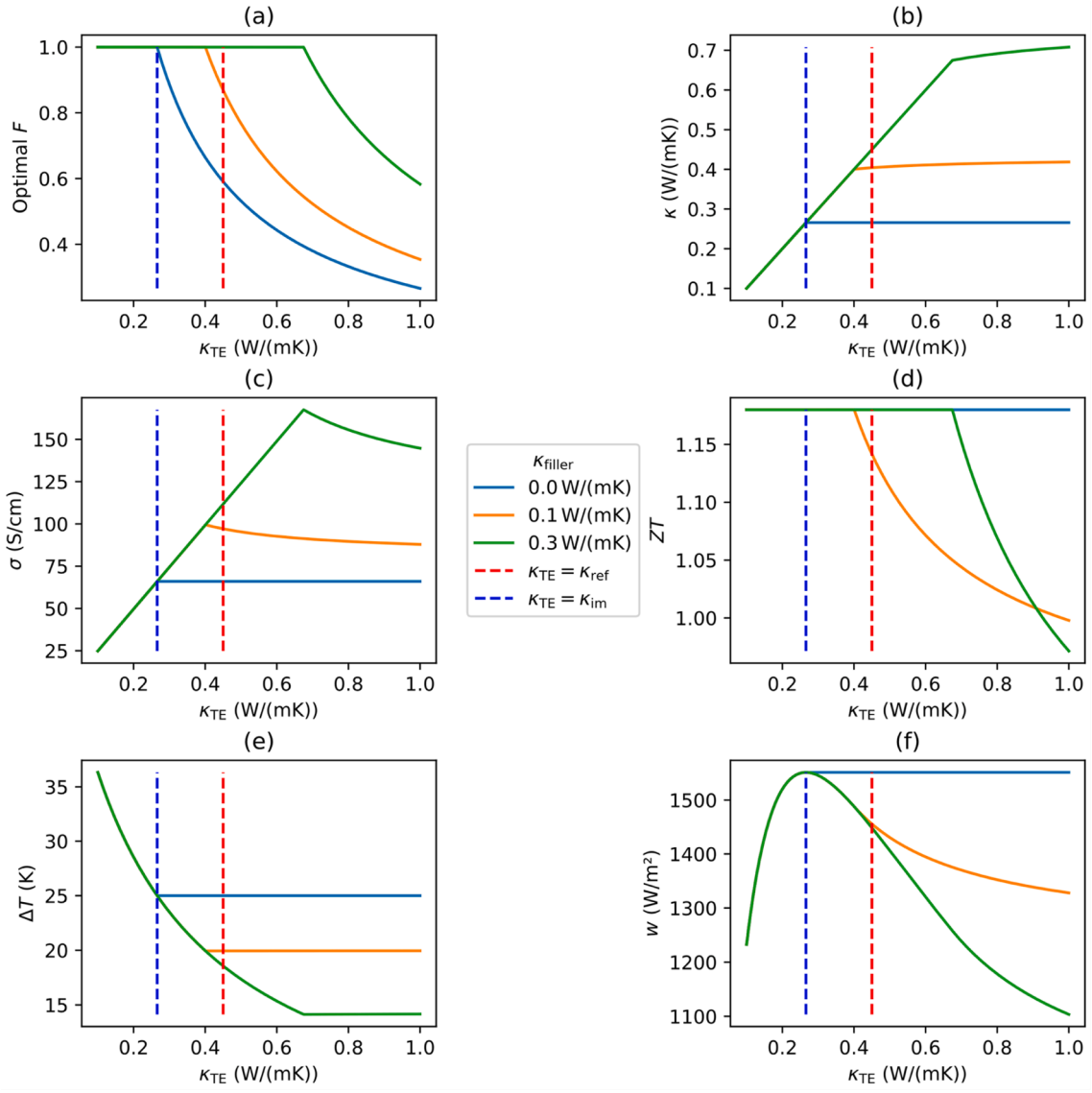

Fig. 7. Device properties of a printed thin film TEG in a heat exchanger application. (a) Numerically optimized fill factor, (b) effective thermal conductivity, (c) effective electrical conductivity, (d) effective device ZT, (e) temperature difference across the device, (f) output power density as a function of the thermal conductivity κ_{TE} of the thermoelectric material.

Lastly, we showed that the selection of the TEG material has to consider the thermal conductivity since two materials with the same zT but different thermal conductivity values can perform differently in devices with geometrically restricted thickness..

Conclusively we can state that while the design and optimization of a TEG has few input parameters, their interdependencies make the analytical optimization very complex and sometimes non-intuitive parameter sets yield the best device performance. Furthermore, it depends on the application and the user for which property the TEG should be optimized, whether it is output power, efficiency, cost per watt ($/W), or levelized cost of energy ($/kWh) or any combination of those. Therefore, we recommend a full digital twin and numerical optimization procedures to design optimum printed thermoelectric generators.

CRediT authorship contribution statement

Andres Georg Rösch: Conceptualization, Writing – original draft, Methodology, Formal analysis. **Leonard Franke:** Resources, Software. **Mofasser Mallick:** Investigation, Data curation. **Uli Lemmer:** Supervision, Project administration, Writing – review & editing.

Declaration of Competing Interest

The authors declare that they have no known competing financial interests or personal relationships that could have appeared to influence the work reported in this paper.

Data availability

Data will be made available on request.

Acknowledgments

The authors wish to acknowledge the Deutsche Forschungsgemeinschaft (DFG, German Research Foundation) under Germanýs Excellence Strategy via the Excellence Cluster 3D Matter Made to Order (EXC-2082/1-390761711) and the BMBF through project 03INT606AG for financial support. The authors wish to acknowledge funding by the Ministry of Science, Research, and Arts of the state of Baden Württemberg through the MERAGEM graduate school. The German Federal Environmental Foundation (Deutsche Bundesstiftung

Umwelt – DBU), through the DBU Ph.D. scholarship program, also supported this work. This project has received funding from the European Union's Horizon 2020 research and innovation program under grant agreement No 814945-SolBio-Rev.

Appendix A. Supplementary material

Supplementary data to this article can be found online at https://doi.org/10.1016/j.enconman.2023.116776.

References

[1] Blair T, Pachauri RK, Pachauri R. Avoiding dangerous climate change. Cambridge University Press; 2006.
[2] Forman C, Muritala IK, Pardemann R, Meyer B. Estimating the global waste heat potential. Renew Sustain Energy Rev 2016;57:1568–79.
[3] Rösch, A. G. *et al.* Fully printed origami thermoelectric generators for energy-harvesting. *npj flexible electronics* **5**, 1–8 (2021).
[4] Burton M, et al. Printed Thermoelectrics. Adv Mater 2022;2108183.
[5] Zang J, et al. Printed flexible thermoelectric materials and devices. J Mater Chem A Mater 2021;9:19439–64.
[6] Wei Q, Mukaida M, Kirihara K, Naitoh Y, Ishida T. Polymer thermoelectric modules screen-printed on paper. RSC Adv 2014;4:28802–6.
[7] Kim J, Kumar R, Bandodkar AJ, Wang J. Advanced Materials for Printed Wearable Electrochemical Devices: A Review. Adv Electron Mater 2017;3:1600260.
[8] Madan D, et al. Dispenser printed circular thermoelectric devices using Bi and Bi 0.5Sb1.5Te3. Appl Phys Lett 2014;104:013902.
[9] Shin S, et al. High-Performance Screen-Printed Thermoelectric Films on Fabrics. Sci Rep 2017;7:7317.
[10] Madan D, Wang Z, Wright PK, Evans JW. Printed flexible thermoelectric generators for use on low levels of waste heat. Appl Energy 2015;156:587–92.
[11] Mallick MM, Franke L, Rösch AG, Lemmer U. Shape-Versatile 3D Thermoelectric Generators by Additive Manufacturing. ACS Energy Lett 2020;6:85–91.
[12] Orrill M, LeBlanc S. Printed thermoelectric materials and devices: Fabrication techniques, advantages, and challenges. J Appl Polym Sci 2017;134:44256.
[13] Seebeck TJ. Ueber die magnetische Polarisation der Metalle und Erze durch Temperatur-Differenz. Annalen der Physik 1826;82:1–20.
[14] Champier D. Thermoelectric generators: A review of applications. Energy Convers Manag 2017;140:167–81.
[15] Jaziri N, et al. A comprehensive review of Thermoelectric Generators: Technologies and common applications. Energy Rep 2019;6:264–87.
[16] Yusuf A, Ballikaya S. Electrical, thermomechanical and cost analyses of a low-cost thermoelectric generator. Energy 2022;241:122934.
[17] Kim, F. *et al.* 3D printing of shape-conformable thermoelectric materials using all-inorganic Bi2Te3-based inks. *Nature Energy 2017 3:4* **3**, 301–309 (2018).
[18] Chen B, et al. Inkjet Printing of Single-Crystalline Bi2Te3 Thermoelectric Nanowire Networks. Adv Electron Mater 2017;3:1600524.
[19] Navone C, Soulier M, Plissonnier M, Seiler AL. Development of (Bi, Sb) 2(Te, Se) 3-based thermoelectric modules by a screen-printing process. J Electron Mater 2010;39:1755–9.
[20] Sarbajna A, Rösch AG, Franke L, Lemmer U, Mallick MM. Inorganic-Based Printed Thermoelectric Materials and Devices. Adv Eng Mater 2022;2200980.
[21] Mallick MM, et al. High Figure-of-Merit Telluride-Based Flexible Thermoelectric Films through Interfacial Modification via Millisecond Photonic-Curing for Fully Printed Thermoelectric Generators. Adv Sci 2022;9:2202411.
[22] Shakouri A. Recent Developments in Semiconductor Thermoelectric Physics and Materials. Annu Rev Mater Res 2011;41:399–431.
[23] Russ B, Glaudell A, Urban JJ, Chabinyc ML, Segalman RA. Organic thermoelectric materials for energy harvesting and temperature control. Nat Rev Mater 2016;1:16050.
[24] Ou C, et al. Fully Printed Organic-Inorganic Nanocomposites for Flexible Thermoelectric Applications. ACS Appl Mater Interfaces 2018;10:19580–7.
[25] Cao Z, Koukharenko E, Tudor MJ, Torah RN, Beeby SP. Screen printed flexible Bi2Te3-Sb2Te 3 based thermoelectric generator. J Phys Conf Ser 2013;476:012031.
[26] Mallick MM, et al. High-Performance Ag-Se-Based n-Type Printed Thermoelectric Materials for High Power Density Folded Generators. ACS Appl Mater Interfaces 2020;12:19655–63.
[27] Wan C, et al. Flexible thermoelectric foil for wearable energy harvesting. Nano Energy 2016;30:840–5.
[28] Suarez F, Nozariasbmarz A, Vashaee D, Öztürk MC. Designing thermoelectric generators for self-powered wearable electronics. Energy Environ Sci 2016;9:2099–113.
[29] Kim SJ, We JH, Cho BJ. A wearable thermoelectric generator fabricated on a glass fabric. Energy Environ Sci 2014;7:1959–65.
[30] Zhang Y, Park SJ. Flexible organic thermoelectric materials and devices for wearable green energy harvesting. Polymers (Basel) 2019;11:909.
[31] Yee SK, Leblanc S, Goodson KE, Dames C. $ per W metrics for thermoelectric power generation: beyond ZT. Energy Environ Sci 2013;6:2561–71.
[32] LeBlanc S, Yee SK, Scullin ML, Dames C, Goodson KE. Material and manufacturing cost considerations for thermoelectrics. Renew Sustain Energy Rev 2014;32:313–27.
[33] Yazawa K, Shakouri A. Optimization of power and efficiency of thermoelectric devices with asymmetric thermal contacts. J Appl Phys 2012;111:1–6.
[34] Yazawa K, Shakouri A. Cost-Efficiency Trade-off and the Design of Thermoelectric Power Generators. Environ Sci Technol 2011;45:7548–53.
[35] Bahk J-H, Fang H, Yazawa K, Shakouri A. Flexible thermoelectric materials and device optimization for wearable energy harvesting. J Mater Chem C 2015;3:10362–74.
[36] Mallick MM, et al. Photonic Curing Enables Ultrarapid Processing of Highly Conducting β-Cu2−δSe Printed Thermoelectric Films in Less Than 10 ms. ACS Omega 2022;7:10695–700.
[37] Mallick MM, et al. Ultra-flexible β-Cu2-δSe-based p-type printed thermoelectric films. Appl Mater Today 2022;26:101269.
[38] Goldsmid, J. *Introduction to Thermoelectricity 2nd edn.* vol. 121 (Springer Nature, 1989).
[39] Yazawa, K., Bahk, J.-H. & Shakouri, A. *Thermoelectric Energy Conversion Devices and Systems.* (2021).
[40] Yazawa K, Shakouri A. Cost-effective waste heat recovery using thermoelectric systems. J Mater Res 2012;27:1211–7.
[41] Nolas, G. S., Goldsmid, H. J., Sharp, J. & Goldsmid, J. *Thermoelectrics : basic principles and new materials developments. Science And Technology* vol. 45 (Springer, 2001).
[42] Yazawa, K. & Shakouri, A. Scalable Cost/Performance Analysis for Thermoelectric Waste Heat Recovery Systems. *Journal of Electronic Materials 2012 41:6* **41**, 1845–1850 (2012).
[43] Mallick MM, et al. Realizing High Thermoelectric Performance of Bi-Sb-Te-Based Printed Films through Grain Interface Modification by an in Situ-Grown β-Cu2-δSe Phase. ACS Appl Mater Interfaces 2021;13:61386–95.
[44] Engineering ToolBox. Heat Exchangers - Heat Transfer Coefficients. https://www.engineeringtoolbox.com/heat-transfer-coefficients-exchangers-d_450.html (2003).
[45] Schmidt KG. Heat ATLAS. VDI Heat Atlas; 2010.
[46] Rösch AG, et al. Improved Electrical, Thermal, and Thermoelectric Properties Through Sample-to-Sample Fluctuations in Near-Percolation Threshold Composite Materials. Adv Theory Simul 2021;2000284.
[47] Jain A, et al. Commentary: The Materials Project: A materials genome approach to accelerating materials innovation. APL Mater 2013;1:011002.
[48] Wang T, Zhang C, Snoussi H, Zhang G. Machine Learning Approaches for Thermoelectric Materials Research. Adv Funct Mater 2020;30:1906041.
[49] Nolas GS, Poon J, Kanatzidis M. Recent Developments in Bulk Thermoelectric Materials. MRS Bull 2006;31:199–205.